A NEUTROSOPHIC APPROACH FOR GLAUCOMA DETECTION IN RETINAL IMAGES

J. SOFIA JENNIFER, T. SREE SHARMILA

Sri Sivasubramaniya Nadar College of Engineering, Kalavakkam, Chennai – 603110, India
Corresponding author: J. SOFIA JENNIFER, E-mail: `sofiajenniferj@ssn.edu.in`

Abstract. In medical world, Glaucoma is a vision threatening retinal disease. This leads to the research scope of detecting glaucoma at early stages for better treatments. Manual approach for detection by ophthalmologists is tiresome and time-consuming, hence an image processing approach of determining the ratio of optic cup with respect to disc (CDR) is focused. This research work proposes a neutrosophic approach for segmentation by transforming the input retinal images to neutrosophic domain. In this neutrosophic approach, the intensity values are represented as truth, indeterminacy and falsity membership. Next, an intensification operation on the resultant images, followed by score function is done to result in a comprehensive outcome. Finally, the clustering technique IFCM is used for segmentation of the optic cup boundary and the optic disc. Experimental result analysis shows that the effectiveness of the proposed methodology is demonstrated since it provides unbiased results of average accuracy of 92.38% on DRISHTI-GS dataset and 91.67% on RIM-ONE dataset.

Key words: cup-to-disc-ratio, glaucoma detection, neutrosophic sets, retinal images, segmentation.

1. INTRODUCTION

Glaucoma is a medical term used for the optic nerve damage leading to permanent loss of vision in later stages. Recently, a study concluded that glaucoma eye disease is the second highest reason for blindness and has affected more than 90 million persons around the world by the year 2020 [1]. Usually, the glaucoma shows no warning signs at early stages but gradually notice a change in vision at advanced stage. Once the optic nerve loses its capabilities, it cannot be recovered and hence an early diagnosis plays a vital role to reduce the progressiveness of eye infections.

Medically, ophthalmologists suggest glaucoma screening by manually determining damaged optic disc. The screening methodology is usually subjective, costly and time consuming thus focusing on image based automatic glaucoma screening [3]. For image-based detection, the difference between the two regions such as optic cup boundary and optic disc boundary needs to be localized separately. In the sample retinal image from Figure 1, the optic cup is the bright yellowish center region, and the outer boundary signifies the optic disc and neuroretinal rim is the layer between optic cup and its boundary [2].

The clinical way of glaucoma detection is to evaluate the cup to disc ratio (CDR). To calculate the CDR, accurate boundary information of both cup and disc is needed. In recent years, there have been better segmentation methods to determine the cup and disc boundary. These approaches have been categorized into model-based and non-model-based approaches [4]. The model-based approaches focus on shape-based template matching, de-formable model, and deep learning model. Numerous studies have been done using deep learning approaches. Y. Jiang [5] uses an end-to-end RCNN method to compute the boundary box and region-of-interest regions. Li [7] proposes the attention-based CNN (AG-CNN) technique for glaucoma recognition. It exhibits good performance and reduces the redundancy of fundus images, but the method depends on the attention prediction subnet. These model-based approaches are time consuming and involve huge data set to improve accuracy.

In a non-model-based approach, image-processing techniques (clustering, thresholding, morphological operations like dilation, closing etc.) are used to extract the optic disc and cup boundary. Wong et al. [8] uses a novel vibrational level set method for optic disc segmentation. Li et al. [9] concentrates on the red channel of the fundus image and this approach is inefficient with the presence of blood vessels. Yu et al. [10] proposes an approach where localization is done using template matching and the blood vessels are removed by a

morphologic filtering. Yin et al. [11] determines the optic disc center and diameter using edge detection and circular Hough transform.

In medical science, the diagnostic image consists of fuzzy and imprecision information that make segmentation and classification a difficult task. Fuzzy concepts are generally used for clustering approach, as their outcomes are more promising. The goal of clustering involves the task of dividing data points into homogeneous groups. J.C. Bezdek et al. [12] proposes a fuzzy clustering algorithm where the prototype of each cluster is a multi-dimensional linear vector, and it uses the statistical method of principal component analysis. Thus, the generalizations of fuzzy sets are generally used to reduce the fuzziness and uncertainty in images but fail to consider the spatial pixel data due to noise and artifacts. To resolve this issue, neutrosophic set is the better way to quantify the images with the usage of indeterminacy. Furthermore, many existing research concludes that segmentation with fuzzy theory holds back more essential information than any state-of-the-art available segmentation methods and hence this is suitable for detailed information in glaucoma detection. Y. Guo [13] proposed a list of fuzzy C-means clustering algorithms, the interval and neutrosophic fuzzy clustering algorithm (NCM) for segmentation. Nimet [14] proposed a novel multiplicative fuzzy regression functions (MFRF) based on the multiplicative fuzzy clustering algorithm to represent fuzzy system modeling. This approach has proved better performance on experimentation analysis. Tongyi [15] uses a new clustering approach by using a local variance template in the non-local spatial information to eliminate the under-segmentation of the non-local spatial information. This approach assigns appropriate weights to each image dimension that improves the segmentation performance of color images.

Our proposed method focuses on using the advantages of neutrosophic sets along with fuzzy clustering with particle swarm optimization to localize the optic cup and disc, as each pixel value is essential to handle data uncertainties to calculate the CDR by categorizing them to truth, indeterminacy, and falsity membership. This idea simplifies the approach leading to less computation time and effort. The rest of the paper is organized as follows: The proposed methodology is explained in Section 2. Section 3 explains the results of the experiment carried out using the proposed method and the conclusion of this work is discussed in Section 4.
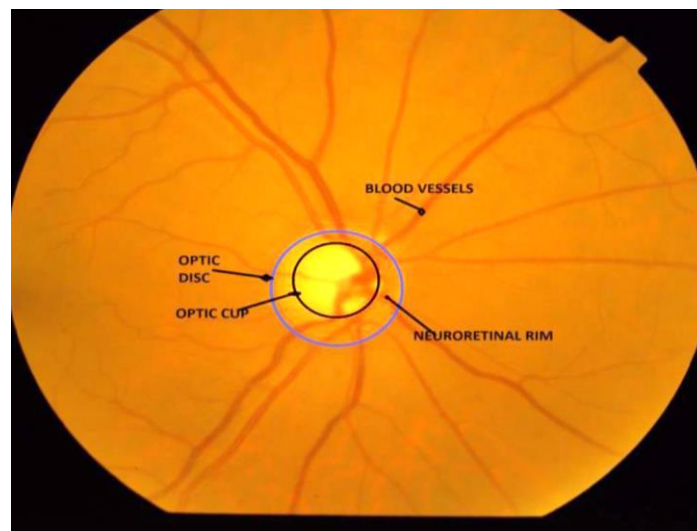

Fig. 1 – Major parts of retinal fundus image.

2. PROPOSED SYSTEM

The proposed system architecture as shown in Fig. 2 consists of the following steps: (i) Neutrosophic domain, (ii) Intensification operation, (iii) Score Function, (iv) IFCM Clustering, (v) Cup to Disc Ratio (CDR). Our proposed system focuses on only the optic cup and the optic disc to extract the accurate boundary information of them. The following steps achieve this: (i) The input retinal image is converted to neutrosophic domain with True (T_T), False (F_T) and Indeterminacy (I_T) set images; (ii) Intensify the T_T, F_T and I_T domain; (iii) Compute the score function of the intensified image; (iv) Perform IFCM clustering on the score image; (v) Segment the optic cup and disc boundary values to calculate CDR for glaucoma detection.
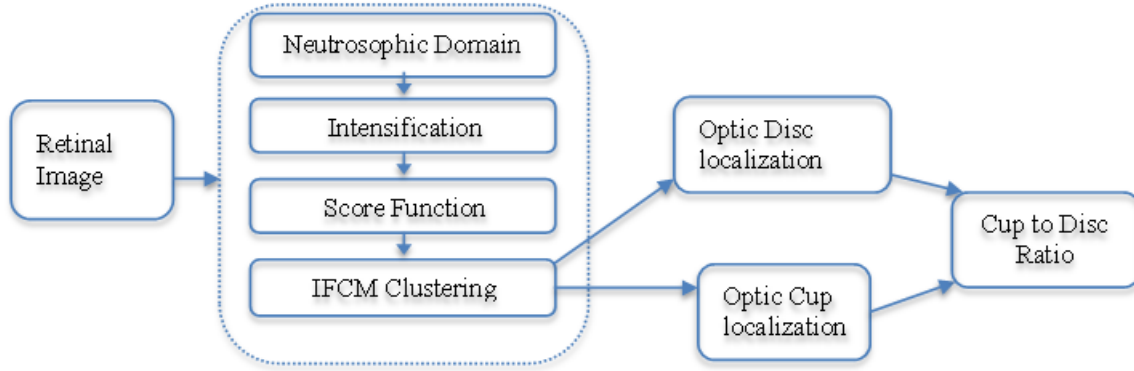
Fig. 2 – Proposed Segmentation architecture.

2.1. Neutrosophic domain

2.1.1. Neutrosophic Set (NS)

Neutrosophy is the study of origin, nature, and scope of neutralities. This is an extended branch of fuzzy logic or set and is generalized as neutrosophic set similarity [16]. The definition, concepts and properties of neutrosophic set (NS) are mentioned in many research papers [17].

Definition. Neutrosophic set (NS): Consider Z to be a universe of discourse. In Z, Neutrosophic set (S) is a part of it. In mathematical terms, an element z in set A is written as $z(t, i, f)$ and represented in NS logic using:

$$S = \left\{ \left[z, \left(T_S(z), I_S(z), F_S(z) \right) \right] z \in Z \right\}, \tag{1}$$

where $T_S(z)$, $I_S(z)$ and $F_S(z)$ are the neutrosophic components and are real standard or non-standard sets of $\left] 0^-, 1^+ \right[$ and is defined using:

$$n_{\sup} = t_{\sup} + i_{\sup} + f_{\sup}, \tag{2}$$

$$n_{\inf} = t_{\inf} + i_{\inf} + f_{\inf}. \tag{3}$$

In Eq. (2), $\sup\_T = t_{\sup}$, $\sup\_I = i_{\sup}$, $\sup\_F = f_{\sup}$ and in Eq. (3), $\inf\_T = t_{\inf}$, $\inf\_I = i_{\inf}$, $\inf\_F = F_{\inf}$ and so $0^- \le T_S(z) + I_S(z) + F_S(z) \le 3^+$.

T, I and F are defined as the degree of the true, indeterminate and false membership function of set A respectively [16]. An element $x(t, i, f)$ belongs to set A and is represented in the following way: t% true, i% indeterminacy, and f% false. In this t varies in T, i varies in I, and f varies in F domain [17].

2.1.2. Images in NS domain

To use Neutrosophic domain in image processing application, initially the image from spatial domain is represented as a neutrosophic image as follows.

Definition 2.1.2. Neutrosophic image (NI): Consider Z to be a universe of the discourse and the image window $W = w * w$ i.e., rows and columns in spatial domain. Thus, W comprises of image intensity pixels, where $W \subseteq Z$ and it holds with bright pixels [13]. As per the Equation 4, the neutrosophic image is generally characterized by membership sets T, I and F [26]. For the proposed image with dimensions $M * N$, each pixel $P_T(m, n)$ is represented as $P_{NS}(m, n)$ in the neutrosophic image. $P_{NS}(m, n)$ interpret the memberships to bright, indeterminate and black intensity values through true $T_T(m, n)$, indeterminate $I_T(m, n)$ and false $F_T(m, n)$ as portrayed in Fig 3a, 3b and 3c respectively. It is represented using [26]:

$$P_{NS}(m, n) = \left\{ T_T(m, n), I_T(m, n), F_T(m, n) \right\}, \tag{4}$$

$$T_T(m, n) = \frac{\overline{g(m,n)} - \overline{g}_{\min}}{\overline{g}_{\max} - \overline{g}_{\min}}. \tag{5}$$

In Equation (5), $\overline{g(m,n)} = \dfrac{1}{w \times w} \sum\limits_{x=m-w/2}^{m+w/2} \sum\limits_{y=n-w/2}^{n+w/2} g(x,y)$. The function $g(x,y)$ is the input retinal image and the parameter window size (w) is dynamically evaluated for values 3, 5 and 7. The value ($w=3$) withholds better results. $\overline{g}_{min}$ and $\overline{g}_{max}$ are the minimum and maximum local mean intensity value of $\overline{g(m,n)}$.

$$I_T(m,n) = \frac{\delta(i,j) - \delta_{min}}{\delta_{max} - \delta_{min}}. \tag{6}$$

In Equation (6), $\delta(m,n) = \text{abs}\left(g(m,n) - \overline{g(m,n)}\right)$ where $g(m,n)$ defines the local mean value of the image. Similarly, minimum and maximum of $\delta(m,n)$ is computed as δ_{min} and δ_{max} respectively.

$$F_T(m,n) = 1 - T_T(m,n). \tag{7}$$

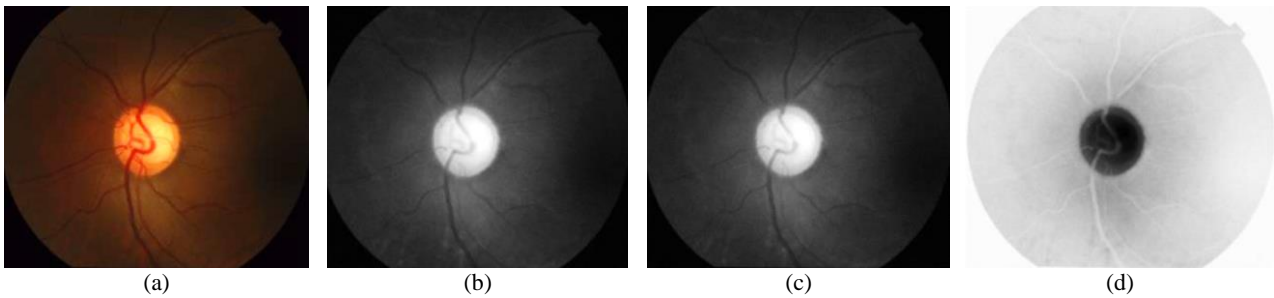(a)   (b)   (c)   (d)

Fig. 3 – a) Input retinal image; b) T_T domain; c) I_T domain, (d) F_T domain.

2.2. Intensification operation

In a pre-processing step, blurring edge features enhances the image. The intensifier operator is applied on T_T, I_T and F_T images to stretch contrast intensity value using [20]:

$$X_{Int}(x,y) = \begin{cases} M \cdot X_T^2(m,n) & \text{if} \quad 0 \leq T_T(m,n) \leq \alpha \\ 1 - 2\left(1 - X_T(m,n)\right)^2 & \text{if} \quad \alpha \leq T_T(m,n) \leq 1. \end{cases} \tag{8}$$

The parameter value of M is assigned within the range 0 to 0.9. An optimal value ($M=0.8$) is chosen based on the better performance. The α value usually ranges within 0 to 1. For experimentation various α values have been worked on, where $\alpha=0.9$ holds promising results by enhancing the images clearer for better segmentation. The distribution of the pixel intensity values in the neutrosophic images becomes more uniform after the intensification operation as depicted in Fig. 4a–4c.
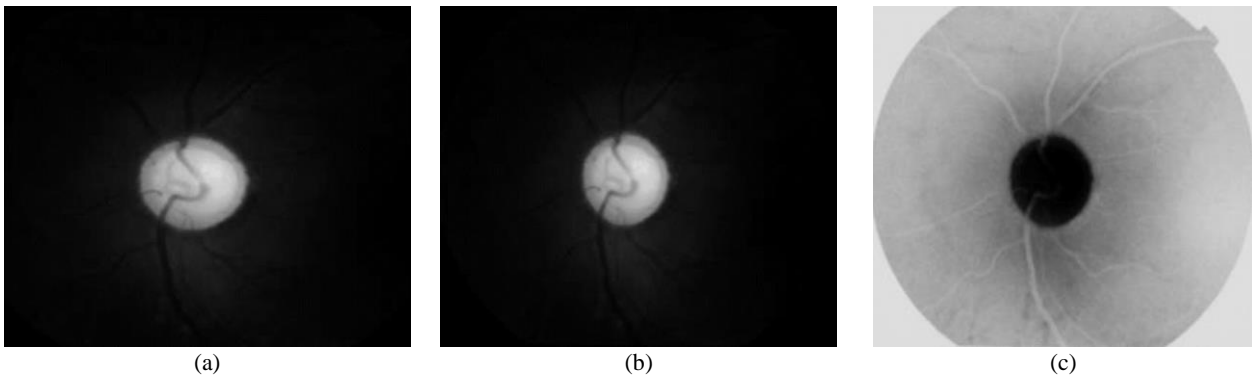

(a)   (b)   (c)

Fig. 4 – Intensification operation: a) T_{Int} domain; b) I_{Int} domain; c) F_{Int} domain.

2.3. Score Function

A score function for single value neutrosophic of pixel intensity values considers the T, I, F degree values. A novel score function is introduced on pixel values to enhance the edge feature points, that provides better segmentation outcomes. Let $A = \{ T_{Int} , I_{Int} , F_{Int} \}$ be the intensified neutrosophic set, the mathematical equation of score function, Score (A) using [20]:

$$\text{Score}(A) = \frac{1}{2} \sum_{t_{Int} \in T_{Int}, \, i_{Int} \in I_{Int}, \, f_{Int} \in F_{Int}} \left(t_{Int} + i_{Int} - f_{Int} \right). \tag{9}$$

In Equation (9), Score (A) is computed using the constraint, $t_{Int} \in T_{Int}$, $i_{Int} \in I_{Int}$ and $f_{Int} \in F_{Int}$.

2.4. Improved Fuzzy C-means (FCM) Clustering Algorithm

In the improved Fuzzy C-means (FCM) clustering approach, initially the cluster size (c) is defined and then the particles are grouped using fuzzy c-means algorithm [23]. As a part of FCM, the metrics used are the Euclidean distance, and an optimal c partition is produced iteratively by minimizing the weighted within group sum of squared error objective function using:

$$f(x_i) = F_m(U, C), \tag{10}$$

$$F_m(U, C) = \sum_{i=1}^{n} \sum_{j=1}^{c} (u_{ij})^m d^2(x_i, c_j), \tag{11}$$

where $X = [x_1, x_2, ..., x_n]$ is the data set in a d-dimensional vector space; n is defined as the number of data items and c is the number of clusters, u_{ij} is the degree of membership of y_i in the jth cluster, m is a weighted exponent on each fuzzy membership, c_j is the center of cluster j and $d^2(x_i, c_j)$ is a square distance measure between object x_i and cluster c_j.

After initial grouping, each particle (x_{ij}) represents where i^{th} particle belongs to j^{th} cluster. The PSO algorithm is based on the group, moving the individual in the group to a good area according to the fitness of the environment. The ith particles of the image data are expressed as $X_i = (x_{i1}, x_{i2}, ..., x_{iD})$, its best position (pbest) is $P_i = (p_{i1}, p_{i2}, ..., p_{iD})$ and the index number of the grouped best position (gbest) is calculated. This approach defines the degree of belonging as neighbors with different degree of neighborhood. For each particle, update the velocity and position using:

$$v_{id}(k+1) = w v_{id}(k) + c_1 \text{rand}_1 \left(\text{pbest}_{id} - x_{id} \right) + c_2 \text{rand}_2 \left(\text{gbest}_{id} - x_{id} \right), \tag{12}$$

$$x_{id}(k+1) = x_{id}(k) + v_{id}(k+1), \tag{13}$$

where, x_{id} are the particles, $v_{id}(k+1)$ is the next iteration velocity, w is an inertial parameter, c_1 and c_2 are acceleration coefficients, rand_1 and rand_2 are random numbers within range 0 to 1.
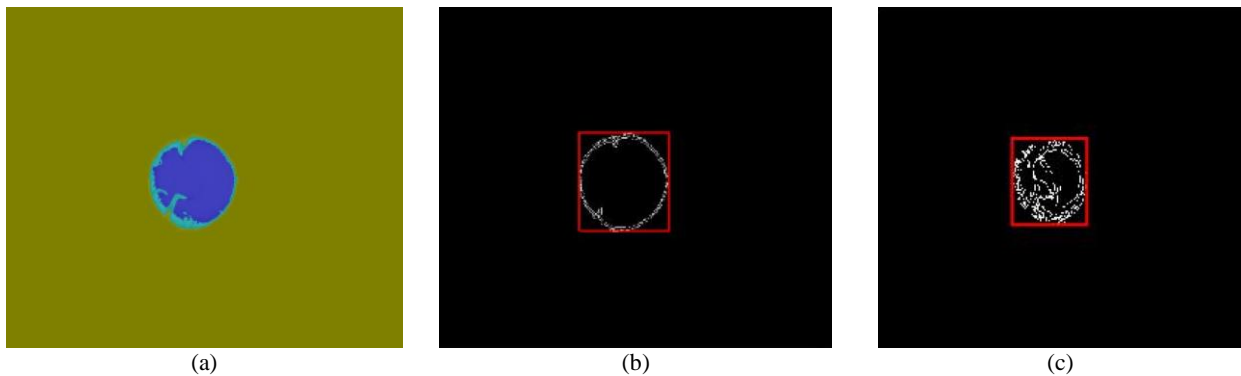

| (a) | (b) | (c) |

Fig. 5 – a) Clustering the neutrosophic image; b) boundary box of optic disc; c) boundary box of optic cup.

Algorithm 1: *IFCM Clustering*
Input: *Score(A) image*
Output: *Segment the retinal image*

i.	Initialize the particles with random positions and velocities on d dimensions in the problem space.
ii.	Cluster the particles using fuzzy c-means clustering algorithm using Equation (10) and (11).
iii.	For each particle, calculate the fitness function (f_i).
iv.	Compare f_i with pbest. If the current value is better than pbest, then set pbest value equal to the current value and the pbest location equal to the current.
v.	Choose the particle with the best fitness value of all particles as gbest.
vi.	For each particle, update the velocity and position using Equation (12) and (13) respectively.
vii.	Repeat the steps (ii)–(vi) until the maximum iterations or minimum error criteria are attained.

This IFCM clustering algorithm for the NS image is applied to the Score(A) as shown in Fig. 5 and explained in Algorithm 1. Then the segmented components are retrieved separately, and the boundary box is drawn over the largest area blob. The boundary box represents the spatial location, the height and the width of the optic cup or disc.

2.5. Cup to Disc Ratio (CDR)

According to medical research, the normal persons have a cup to disc ratio is about 1/3 or 0.3 [21]. The higher the CDR value is directly propositional to the severity chance of vision loss. The CDR value is computed as vertical cup diameter (VCD) to vertical disc diameter (VDD) using:

$$CDR = \frac{VCD}{VDD}. \tag{14}$$

Vertical cup and disc diameter is extracted from the height of the boundary box. If the CDR output is greater than 0.3, then it is considered to be glaucomatous otherwise healthy.

Algorithm 2: *Glaucoma Detection*
Input: *Input data from open-source dataset*
Output: *(i) Localize the optic disc and cup from input image*
(ii) Glaucoma or normal detection

i.	Input the image from the open-source dataset.
ii.	Transform the input retina image to Neutrosophic domain using Equation (4) where T_T, I_T and F_T are calculated using Equation (5), (6) and (7) respectively.
iii.	Enhance using Intensification operation on each neutrosophic set images from (T_T, I_T, F_T) to (T_{Int}, I_{Int}, F_{Int}) using Equation (8).
iv.	Apply a score function Score(A) on the intensified image (T_{Int}, I_{Int}, F_{Int}) using Equation (9).
v.	Segment the Score(A) image using Algorithm 1 (IFCM Clustering).
vi.	Draw the boundary box on the largest blob of the segmented image to determine the height and width of optic cup and disc.
vii.	Calculate the CDR based on vertical cup and vertical disc using Equation (14).
viii.	If CDR > 0.3, Glaucoma is detected; Otherwise, it is considered as normal.

3. EVALUATION

3.1. Datasets

For retinal image acquisition, the rear images of the eye are captured using fundus camera for glaucoma detection. The fundus camera available in eye care hospitals usually captures the eye components such as optic disc, optic cup, fovea, exudates retina, and macula [22]. The proposed work has used two open datasets, such as DRISHTI-GS [19] and RIM-ONE [24], to validate the effectiveness of the neutrosophic domain. The DRISHTI-GS dataset [19] holds a total of 101 images containing 31 normal images and 70 glaucomatous images in $2\,896 \times 1\,944$ resolutions. The RIM-ONE r2 dataset [24] contains 455 retinal fundus images with 255 normal images and 200 glaucoma images. The experimental code is available in github repository.

3.2. Performance measures

3.2.1. Dice co-efficient (DICE)

DICE is a performance measure used to quantify the segmentation approach. It computes the extent of overlapping pixel values between any two images that takes the segmentation area and the background with respect to the ground truth segmentation [27]. The Dice coefficients are defined using:

$$\text{DICE} = \frac{2 \times N_{\text{TP}}}{2 \times N_{\text{TP}} + N_{\text{FP}} + N_{\text{FN}}}, \tag{15}$$

where N_{TP} is the number of true positive, N_{FP} and N_{FN} is the is the number of false positive and false negative respectively. The positive and negative term refers to the pixels belonging to the optic cup/disc area and background area in comparison with ground truth.

3.2.2. Boundary localization error (BLE)

In optic cup and disc detection task, for each candidate window, the offset between the calculated and the closest ground truth (top, side, height, and width of boundary boxes) are predicted. The learning objective is formulated as a regression problem and the boundary localization error for the samples is calculated using [25]:

$$L_i^{\text{box}} = \| \hat{y}_i^{\text{box}} - y_i^{\text{box}} \|^2, \tag{16}$$

where $\hat{y}_i^{\text{box}}$ is the original coordinate position of the optic cup or disc and y_i^{box} is the resultant four coordinates including top, side, height and width based on Algorithm 1.

3.2.3. Accuracy

The accuracy of the segmentation using neutrosophic approach to detect glaucoma or not is computed on the datasets using [26]

$$\text{Accuracy} = \frac{\text{TP} + \text{TN}}{\text{TP} + \text{TN} + \text{FP} + \text{FN}}. \tag{17}$$

3.2.4. Root mean square error (RMSE)

This measure gives the difference between the source image and the segmented image [18] and is represented using:

$$\text{RMSE} = \sqrt{\frac{\sum_{i=1}^{m} \sum_{j=1}^{n} \left[M(i,j) - F(i,j) \right]^2}{m \times n}}, \tag{18}$$

where m and n are the size of the image, i and j are the pixel positions in the image, $M(i,j)$ is the segmented image and $F(i,j)$ is the Score(A) image. The smaller the value of RMSE, the better the segmentation performance.

3.2.5. Peak signal to noise ratio (PSNR)

PSNR is defined as the ratio between the maximum value of an image and the value of background noise [26]. The PSNR in terms of RMSE is defined using:

$$\text{PSNR} = 10 \times \ln \left(\frac{f_{max}}{\text{RMSE}} \right)^2, \tag{19}$$

where $f_{\max}$ is the maximum value of pixels in the segmented image. Higher the PSNR value, better the segmentation performance.

3.3. Experimental results

The proposed system uses the neutrosophic approach followed by IFCM clustering for glaucoma detection. The IFCM clustering uses PSO to focus on to find the particle position that results in best evaluation of fitness function. The PSO based clustering reduces the effect that initial condition possess when compared to k-means clustering and the algorithm. The initial parameter settings of PSO are defined in Table 1.

Table 1

Parameters and its value of PSO

Parameters	Values
Swarm size	250
Iteration	50
Inertia	1.0
Function tolerance	1.000 e–06
Maximum time	50
Maximum stall time	500×number of variables
Number of variables	4

The improved Fuzzy clustering approach with PSO is compared with the state-of-the-art clustering algorithms like k-means, improved K-means and FCM for segmentation in Table 2. Performance analysis table reveals that the RMSE and PSNR values of improved fuzzy c-means provide better results. On execution the major issue faced is the execution time as the average time of IFCM is higher than k-means and FCM.

Table 2

Performance evaluation of different clustering methods for segmentation

Clustering Methods	RMSE	PSNR	TIME (s)
K-means	0.063	32.80	1.21
Improved K-means	0.054	35.73	1.98
FCM	0.042	36.45	2.12
Improved FCM	0.023	38.321	2.243

The proposed glaucoma detection system uses the performance metrics DICE, BLE and accuracy to compare with the other existing approaches available in market such as Superpixel [3], LSACM [6], LSACM-SP [22] and FDMT [10] using Equation (15)–(17) is tabulated in Table 3 on DRISHTI-GS and RIM-ONE database. Figure 6 portrays few samples of cup and disc segmentation from DRISHTI-GS and RIM-ONE datasets. The tables below compare few available state-of-the-art approaches in both datasets to justify the effectiveness of the proposed segmentation approach. For BLE, the relative error measure ($L_i^{\text{box}} \leq 0.05$) is considered for comparison.

Table 3

Optic cup and disc segmentation results on DRISHTI-GS and RIM-ONE

Methods	DRISHTI-GS			RIM-ONE		
	DICE	BLE	ACCURACY	DICE	BLE	ACCURACY
Superpixel [3]	0.932	75.4%	69.27	0.816	75.4%	78.64
LSACM [6]	0.931	79.2%	88.63	0.808	79.2%	80.18
LSACM-SP [22]	0.955	82.2%	89.01	0.853	82.2%	84.46
FDMT [10]	0.85	85.7%	90.2	0.85	85.7%	87.12
Proposed Neutrosophic	**0.972**	**93.5%**	**92.38**	**0.917**	**93.5%**	**91.67**
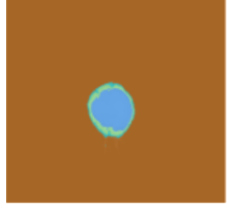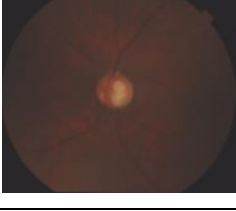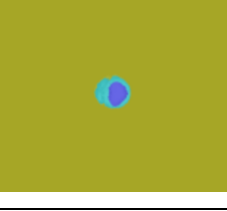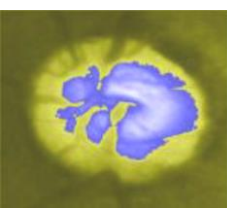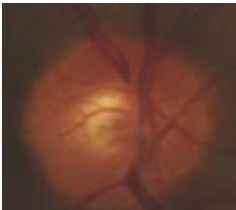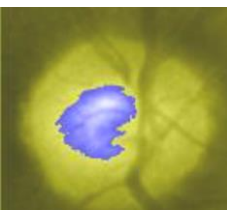
Database	Glaucoma/Normal	Input Image	Segmented Image
DRISHTI-GS	Glaucoma		
DRISHTI-GS	Normal		
RIM-ONE	Glaucoma		
RIM-ONE	Normal		

Fig. 6 – Segmented optic disc and cup on sample images of DRISHTI-GS and RIM-ONE database.ö.

4. CONCLUSION

Glaucoma eye disease on latter stages is irreversible and leads to permanent vision loss. Hence, early detection of glaucoma has become vital research. The glaucoma CDR is evaluated using the vertical diameter of optic cup and disc. To segment the cup and disc separately, the proposed work focuses on novel neutrosophic segmentation approach. Initially the input images are forwarded to a neutrosophic framework and intensified to promote better segmentation results. Then, the final images are combined using score function and segmented using clustering. The proposed approach is tested on two open datasets namely DRISHTI-GS and RIM-ONE r2, and demonstrate that the neutrosophic method consistently outperform the state-of-the-art methods. In future work, more focus is needed on developing a graphical user interface that allows ophthalmologist work on an automatic tool for diagnosis.

REFERENCES

1. Y. GAO, X. YU, C. WU, W. ZHOU, X. WANG, H. CHU, *Accurate and efficient segmentation of optic disc and optic cup in retinal images integrating multi-view information*, IEEE Access, **7**, *1*, pp. 148183–148197, 2019.
2. H.A. QUIGLEY, A.T. BROMAN, *The number of people with glaucoma worldwide in 2010 and 2020*, British Journal of Ophthalmology, **90**, *3*, pp. 262–267, 2006.

3. J. CHENG, J. LIU, Y. XU, F. YIN, D.W.K. WONG, N.M. TAN, D. TAO, C.Y. CHENG, T. AUNG, T.Y. WONG, *Superpixel classification based optic disc and optic cup segmentation for glaucoma screening*, IEEE Transactions on Medical Imaging, **32**, *6*, pp. 1019–1032, 2013.

4. M.S. HALEEM, L. HAN, J.V. HEMERT, B. LI, A. FLEMING, L.R. PASQUALE, B.J. SONG, *A novel adaptive deformable model for automated optic disc and cup seg- mentation to aid glaucoma diagnosis*, Journal of Medical Systems, **42, 1**, art. 20, 2018.

5. Y. JIANG, L. DUAN, J. CHENG, Z. GU, H. XIA, H. FU, C. LI, J. LIU, *JointRCNN: a region-based convolutional neural network for optic disc and cup segmentation*, IEEE Transactions on Biomedical Engineering, **67**, *2*, art. 2913211, pp. 335–343, 2019.

6. R. PRIYADHARSINI, A. BEULAH, T. SREE SHARMILA, *Optic disc and cup segmentation in fundus retinal images using feature detection and morphological techniques*, Current Science, **115**, *4*, pp. 748–752, 2018.

7. L. LI, *A large-scale database and a CNN model for attention-based glaucoma detection*, IEEE Transactions on Medical Imaging, **39**, *2*, pp. 413–424, 2019.

8. D.K. Wong, J. Liu, J.H. Lim, *Level-set based automatic cup-to-disc ratio determination using retinal fundus images*, ARGALI. Conf. Proc. IEEE Eng. Med. Biol. Soc., 2008, pp. 2266–2269.

9. C. Li, C. Xu, C. Gui, M.D. Fox, *Level set evolution without re-initialization: a new variational formulation*, Proceedings of the IEEE Computer Society Conference on Computer Vision and Pattern Recognition, San Diego, CA, USA, 2005, Vol. 5, pp. 430–436.

10. H. Yu, E.S. Barriga, C. Agurto, *Fast localization and segmentation of optic disk in retinal images using directional matched filtering and level sets*, IEEE Trans. Inf. Technol. Biomed., **16**, *4*, pp. 644–657, 2012.

11. F. YIN, J. LIU, S.H. ONG, *Model-based optic nerve head segmentation on retinal fundus images*, Conf. Proc. IEEE Eng. Med. Biol. Soc., 2011, pp. 2626–2629.

12. J.C. BEZDEK, C. CORAY, R. GUNDERSON, J. WATSON, *Detection and characterization of cluster substructure i. linear structure: Fuzzy c-lines*, SIAM Journal on Applied Mathematics, **40**, *2*, pp. 339−357, 1981.

13. Kuei-Hu CHANG, *A novel risk ranking method based on the single valued neutrosophic set*, Journal of Industrial & Management Optimization, **18**, *3*, pp. 2237−2253, 2022.

14. Nimet YAPICI PEHLIVAN, Ismail Burhan TURKSEN, *A novel multiplicative fuzzy regression function with a multiplicative fuzzy clustering algorithm*, Romanian Journal of Information Science and Technology, **24**, *1*, pp. 79–98, 2021.

15. Tongyi WEI, Xiaopeng WANG, Xinna LI, Shengyang ZHU, *Fuzzy subspace clustering noisy image segmentation algorithm with adaptive local variance & non-local information and mean membership linking*, Engineering Applications of Artificial Intelligence, **110**, art. 104672, 2022.

16. F. SMARANDACHE, *A unifying field in logics: Neutrosophic logic*, Multiple-Valued Logic**, 8**, pp. 489–503. 1999.

17. F. SMARANDACHE, *A unifying field in logics: Neutrsophic logic, neutrosophy, neutrosophic set, neutrosophic probability* (Fourth edition), University of New Mexico, **332**, pp. 5–21, 2002.

18. A. SEVASTOPOLSKY, *Optic disc and cup segmentation methods for glaucoma detection with modification of U-Net con- volutional neural network*, Pattern Recognition and Image Analysis, **27**, *3*, pp. 618–624, 2017.

19. J. SIVASWAMY, S.R. KRISHNADAS, G.D. JOSHI, M. JAIN, A.U.S. TABISH, *Drishti-GS: retinal image dataset for optic nerve head (ONH) segmen- tation*, International Symposium on Biomedical Imaging, Beijing, China, April 29 – May2, 2014, Proceedings of the IEEE, pp. 53–56.

20. Ye YUAN, Yan REN, Xiaodong LIU, Jing WANG. *Approach to image segmentation based on interval neutrosophic set*, Numerical Algebra, Control & Optimization, **10**, *1*, pp.1-11, 2020.

21. F. YIN, J. LIU, D. W. K. WONG, N.M. TAN, C. CHEUNG, M. BASKARAN, T. AUNG, T.Y. WONG, *Automated segmentation of optic disc and optic cup in fundus images for glaucoma diagnosis*, Proc. of International Symposium on Computer-Based Medical Systems, Rome, Italy, June 2012, Vol. 54, pp. 1–6, 2012.

22. Wei ZHOU, Yugen YI, Yuan GAO, Jiangyan DAI, *Optic disc and cup segmentation in retinal images for glaucoma diagnosis by locally statistical active contour model with structure prior*, Computational and Mathematical Methods in Medicine, art. 8973287, 2019.

23. N.K. NAGWANI, S.V DEO, *Estimating the concrete compressive strength using hard clustering and fuzzy clustering based regression techniques*, The Scientific World Journal, art. 381549, 2014.

24. F. FUMERO, S. ALAYON, J. L. SANCHEZ, J. SIGUT, AND M. GONZALEZ- HERNANDEZ, *RIM-ONE: an open retinal image database for optic nerve evaluation*, Proceedings of the 24th In- ternational Symposium on Computer-Based Medical Systems (CBMS), IEEE, Bristol, UK, pp. 1–6, June 2011.

25. M. ZHANG, L. ZHANG, H.D. CHENG, *A Neutrosophic approach to image segmentation based on Watershed method*, Signal Processing, **90**, *5*, pp. 1510–1517, 2010.

26. J. SOFIA JENNIFER, T. SREE SHARMILA, *Real time blink recognition from various head pose using single eye*, Multimedia Tools and Applications, **77**, pp. 31331−31345, 2018.

27. J. SOFIA JENNIFER, T. SREE SHARMILA, R. SRINIVASAN, *Facial feature extraction for head tilt images based on eye canthus*, IEEE TENCON, **1**, pp. 566−570, 2016.